Arabian Journal of Chemistry (2021) **14**, 103202

King Saud University

Arabian Journal of Chemistry

www.ksu.edu.sa
www.sciencedirect.com

ORIGINAL ARTICLE

Cellulose-based catalyst design for efficient chlorate reduction

Emőke Sikora [a,*], Kitti Krisztina Katona [a], Gábor Muránszky [a], Olivér Bánhidi [a], Ferenc Kristály [b], József T. Szabó [c], Márk Windisch [c], Béla Fiser [a,d], László Vanyorek [a]

[a] *Institute of Chemistry, University of Miskolc, Hungary*
[b] *Institute of Mineralogy and Geology, University of Miskolc, Hungary*
[c] *Bay Zoltán Nonprofit Ltd. for Applied Research Engineering Division (BAY-ENG), Department of Industrial Materials Technology, Hungary*
[d] *Ferenc Rákóczi II. Transcarpathian Hungarian Institute, Ukraine*

Received 11 March 2021; accepted 2 May 2021
Available online 11 May 2021

KEYWORDS

Cellulose;
Catalyst;
Chlorate reduction;
Catalytic hydrogenation

Abstract The reduction of undesirable chlorate (ClO_3^-) is important from both an environmental and an industrial point of view. In our work, cellulose-based catalysts have been designed for chlorate reduction by using palladium, platinum, and iron oxide. The produced catalysts were characterized by SEM, TEM, XRD, FTIR, and ICP. Even though low precious metal content (< 0.6 wt %) was used during the catalyst preparation, high catalytic activity was achieved, and the conversion was as high as 92.5%. Furthermore, a continuous chlorate hydrogenation and monitoring system has also been developed within which the reduction has been carried out successfully and after about 160 min the ClO_3^- content has been reduced to zero.

1. Introduction

During water disinfection processes or chloralkali electrolysis, the formation of toxic species such as chlorate (ClO_3^-) occurs. The reduction of such undesirable species is important from both an environmental and an industrial point of view (Brinkmann et al., 2014; Jakab-Nácsa et al., 2020; Ren et al., 2020; WHO, 2005). Due to a side reaction during chloralkali electrolysis, oxygen is formed at the anode and chlorate at the anolyte. Thus, brine is produced which is contaminated with chlorate, but recycled in the process. However, the chlo-

* Corresponding author.
E-mail address: emoke.sikora@gmail.com (E. Sikora).
Peer review under responsibility of King Saud University.

Production and hosting by Elsevier

https://doi.org/10.1016/j.arabjc.2021.103202

rate contamination will reduce the quality of caustic soda and could damage the equipment which will further decrease the efficiency of the procedure (Brinkmann et al., 2014). It is important to implement a prevention-, reduction-, and/or post-treatment into the process which could effectively reduce the amount of the above mentioned by-product (Brinkmann et al., 2014; Maslamani et al., 2020). In chloralkali plants, the commonly used method is thermal hydrochloric acid treatment, which is energy- and chemical-intensive (about 90 °C, pH 0, conversion 60–90%) (Ren et al., 2020). In contrast to this, by applying a suitable catalyst, less chemicals and energy is necessary and higher conversion could be achieved during a heterogeneous catalytic hydrogenation and the hydrogen which is formed during the electrolysis can also be used (Brinkmann et al., 2014; Ren et al., 2020).

Recently carbon supported platinum group metal (Pd, Pt, Ru, Ir, Rh) catalysts were tested in the catalytic hydrogenation of chlorate with promising results (Chen et al., 2017; Kuznetsova et al., 2012; Rutger et al., 2001). However, such powder-based catalysts have a disadvantage, as their separation from the reaction medium is difficult. It is preferable for industrial applications, especially in flow catalytic processes to use macroscopic structured materials (Akhtar et al., 2014) such as zeolites (Yilmaz and Müller, 2009) and monoliths (Hosseini et al., 2020), because they are easy to handle.

Due to environmental issues, there has been an increasing focus on renewable and degradable raw carbon based materials (Nasrollahzadeh et al., 2020). Cellulose is a good example of such materials which is widely available, inexpensive, and nontoxic and thus, its potential application in the field of heterogeneous catalysis is intensively researched (Xie et al., 2019). Cellulose-supported catalysts have been tested with great success in case of various chemical transformations including the Suzuki reaction (Dong et al., 2020), cycloaddition (Bahsis et al., 2018), degradation of methyl orange (Tavker et al., 2020), nitrobenzene (Li et al., 2020), p-nitrophenol (Lin et al., 2011; Wu et al., 2013) and methylene blue reduction (Wu et al., 2013).

Several efficient cellulose supported noble metal catalysts have been developed (Dong et al., 2020; Li et al., 2013). Gold nanoparticle-cysteamine/carboxymethyl cellulose (Tan et al., 2010) and cellulose nanocrystal-supported gold nanoparticles (Wu et al., 2014) have also been created before. Furthermore, controlled shape Pt nanoparticles with high catalytic activity have been prepared by using wood nanomaterials (Lin et al., 2011). Palladium nanoparticles on modified cellulose support have been utilized as catalyst in the hydrodeoxygenation of vanillin (Li et al., 2018). Flow-through catalytic experiments have also been performed, by using Au containing (Xie et al., 2020, 2019) or hybrid CNF/TiO_2 (Lucchini et al., 2018) cellulose monoliths. These systems are not only efficient catalysts, but their production can be carried out in a green and environmentally friendly way (Wu et al., 2014; Li et al., 2013; Quignard and Choplin, 2001).

In this research, cellulose beads (CB) have been used as support material in the design of palladium and platinum catalysts for catalytic hydrogenation of chlorate. The catalysts have been tested in both batch and continuous flow reactors. The effect of Fe_2O_3 as catalyst promoter has also been studied, because previously it was shown that the (per)chlorate content of brine can be reduced by using iron combining it with UV light (Gurol and Kim, 2003).

2. Experimental

2.1. Materials

Iron(III) oxide (Fe_2O_3, Reanal), palladium(II) nitrate dihydrate ($Pd(NO_3)_2$•2 H_2O, Alfa Aesar) and Platinum(IV) chloride ($PtCl_4$, Reanal), and hydrazine monohydrate ($H_4N_2{\cdot}H_2O$, Alfa Aesar) were used for the catalyst preparation. Cellulose beads (Magyar Viscosagyár), semi-synthetic spherical material was used as catalyst support. The applied cellulose support is well wettable, swell in an aqueous environment, absorb water, and can also absorb metal salt solutions well, which is the reason why it was chosen in the current study. Potassium-chlorate ($KClO_3$, Aldrich), potassium-iodide, (KI, Merck), concentrated hydrochloric acid (37 wt %, HCl, VWR), sulfuric acid (95 wt%, H_2SO_4, VWR), hydrogen and nitrogen (5.0 and 4.5 purity, Messer Ltd.) were used during the chlorate hydrogenation experiments.

2.2. Catalyst preparation method

As a first step, palladium and platinum containing solution was prepared with 0.8 g/L concentration. The ratio of the noble metals was 7:1 in both samples (*e.g.* 0.7 g/L Pd and 0.1 g/L Pt or vice versa). The name of the catalysts indicates the ratio of precious metals, and thus, the solution which contained more palladium is called as Pd-Pt and while the one with more platinum is referred to as Pt-Pd. To a 100 ml solution, 2 g of cellulose beads were added and treated with ultrasonic Hielscher homogenizer for 5 min. Then 2 ml of hydrazine monohydrate (98 wt%) as reducing agent was added dropwise with stirring. Dispersion containing 3 g/L Fe_2O_3 in a volume of 100 ml was prepared and added after reduction as a promoter in two cases, and this was followed by ultrasonic homogenization. Finally, the samples were dried using a vacuum evaporator and then, in an oven at 105 °C overnight.

2.3. Characterization techniques

The particle size and morphology of the catalysts were studied by high-resolution scanning electron microscope (SEM) applying a Helios G4 PFIB CXe (Thermo Scientific) instrument, using carbon tape for sample preparation. To achieve a higher resolution, a JEOL JSM-IT700HR-LA electron microscope was also applied, and it did not required specific sample preparation.

To characterize the catalysts high-resolution transmission electron microscopy was also applied (HRTEM) by using the FEI Technai G2 equipment (electron source W emitter, 200 kV). Sample preparation was carried out by dropping aqueous suspension of the powdered catalysts on 300 mesh copper grids (lacey carbon, Ted Pella Inc.). The diameters of the nanoparticles were measured on the HRTEM images based on the original scale bar by using the ImageJ software.

X-ray powder diffraction measurements were carried out by using a Bruker D8 Discover instrument (Cu K-alpha, 40 kV and 40 mA) in a parallel beam geometry obtained with Göbel mirror. For the measurements, a 0.2° equatorial Soller slit and LynxEye X-ET energy dispersive detector in 0D and high-resolution mode was used. Patterns were recorded in

the 2–100°(2Θ) angular region with 0.01°(2Θ)/124 sec counting time. The recorded patterns were evaluated by Pawley (single peak) fitting in the TOPAS4 software with instrumental convolution determined on NIST SRM 640d Si powder and by using 4th degree Tschebyshev polynomial background which was determined on the Si standard.

BET specific surface area of the catalyst samples has also been determined by using N_2 with a Micrometics TriStar 3000 instrument.

The functional groups located on the catalysts were identified by using a Bruker Vertex 70 Fourier-transform infrared spectroscope (FTIR, detection range was 500–4000 cm^{-1} at 4 cm^{-1} optical resolution).

The metal content of the catalysts was analyzed by a Varian 720 ES inductively coupled optical emission spectrometer (ICP-OES) using Merck Certipur ICP multi-element standard IV. The sample preparation began with heat treatment at 800 °C, and then, the combustion residue was dissolved in a 3:1 mixture of hydrochloric acid and nitric acid at 200 °C.

2.4. Hydrogenation tests

2.4.1. Hydrogenation in batch reactor

The measurements were performed in a side-inlet gas washing bottle with fritted disc which was placed in a Julabo circulator. The hydrogenation of aqueous solution of potassium chlorate (Eq. (1)) (100 ml, 200 mg/dm^3) was carried out at 80 °C, with 40 sccm nitrogen and 100 sccm hydrogen. In each case 1 g catalyst was used. The experiments lasted for 3 h and sampling was carried out after 0, 5, 15, 30, 45, 60, 90, 120, 150, and 180 min. For each sample (1 ml) 0.1 g potassium iodide and 1 ml hydrochloric acid were added and then, it was diluted to 50 ml with distilled water to apply redox reaction (Eq. (2)).

$$ClO_3^- + 3H_2 \rightarrow Cl^- + 3H_2O \quad (1)$$

$$KClO_3 + 6KI + 6HCl \rightarrow 3H_2O + 3I_2 + 7KCl \quad (2)$$

Thus, iodine formed in proportion to the chlorate concentration and appears with yellow colour in the solution. This colour change was followed with UV-6300PC spectrophotometer at 351 nm wavelength. The spectrophotometric method was calibrated by using potassium chlorate solutions with different concentrations (0, 50, 100, 150 and 200 mg/dm^3).

2.4.2. Hydrogenation in a continuous flow system

wThe aqueous solution of potassium chlorate (200 mg/dm^3) was flowed through the reactor (Fig. 1.) controlled by a peristaltic pump (0.5 ml/min). The reaction was performed at 80 °C, and the hydrogen flow rate was 100 ml/min, while 6 g catalyst was used. The hydrogenated solution is transferred by the pump to a branch where aqueous solution of potassium iodide (28 g/dm^3) and sulfuric acid (4.5 mol/dm^3) were added. As in the batch hydrogenation, iodine was formed in proportion to the chlorate concentration (Eq. (2)). The iodine containing solution was transmitted to the spectrophotometric measuring cell and the colour change was used to follow the concentration of chlorate.

In order to monitor the chlorate concentration continuously, a special spectrophotometric cell was constructed (Fig. 1) which consisting of a flowthrough cell, a light source and a light sensor.

The cell is a square cross-section cuvette with input and output openings. Although the absorption maximum of I_3^- ion in aqueous media is about 353 nm, the molar absorption coefficient is high enough at the emission maximum of a UV LED (~380 nm) to be able to measure and follow the changes of the chlorate concentration without applying a dedicated monochromator unit. Therefore, a UV LED and a phototransistor were used as a light source and a detector, respectively. The light source and the detector were placed on the opposite side of the cell at the same height. In this way a rather compact device has been developed with a small sample volume (~2 cm^3) which led to a short dead time necessary to detect any change in the concentration. The applied LED was operated with a current generator to achieve stable emission intensity. The collector electrode of the phototransistor was connected to a power supply (+9V), while the base electrode was not connected to any voltage, so no bias base-voltage was applied. However, the light sensitivity decreased, and therefore no electric signal could be measured at daylight illumination at the connecting point, the loading resistor, and the emitter electrode of the transistor. Despite the reduced sensitivity, the emission of the LED produced a sufficient output signal to carry out measurements in the 1–250 mg/dm^3 concentration range.

The output signal was led to an AD converter (ADC Protoboard, manufactured by Mikroelectronica Ltd.), which was connected to a Raspberry Pi B card (credit-card-size ARM-based computer, manufactured by Raspberry Pi Foundation). As an operating system, a special Linux distribution, Raspbian was used. A special measuring and monitoring program was written to carry out the necessary tasks, such as the calibration and recalibration of the system, continuous monitoring of the chlorate concentration and recording the data.

3. Results and discussion

Four different palladium and platinum containing, cellulose bead (CB) supported catalysts, Pd-Pt/CB-Fe_2O_3, Pt-Pd/CB-Fe_2O_3, Pd-Pt/CB, and Pt-Pd/CB have been successfully prepared. Iron oxide have been used as a promoter material in two cases, and the specific surface area of these samples is about two times larger (Pd-Pt/CB-Fe_2O_3: 0.4177 m^2/g and Pt-Pd/CB-Fe_2O_3: 0.5212 m^2/g) than in the case of their counterparts (Pd-Pt/CB: 0.2124 m^2/g and Pt-Pd/CB: 0.1937 m^2/g).

Pd and Pt aggregates have been located on the surface of the cellulose beads (Fig. 2.). In the case of the iron oxide containing samples, the surface is richly covered with the promoter as well (Fig. 2, A and B).

On the SEM images, nanoparticles are visible with a diameter of a few tens of nanometres (SI Fig. 1). However, due to the lower resolution of the SEM, particles with < 10 nm diameter can not be located, thus, to get a better resolution, the nanoparticles have been detached from surface of the cellulose beads and these were examined by HRTEM. On the HRTEM images of the catalysts (SI Fig. 2) palladium and platinum nanoparticles have been identified. There is no significant difference between the size of the nanoparticles in the different samples. In each case, the particles are < 10 nm and their average size is ~4.9 nm. It was also confirmed by XRD measurements, that the size of the Pd and Pt nanoparticles is about 10 nm, and the anatase particles are 45 nm, while the hematite particles are bigger than 100 nm.

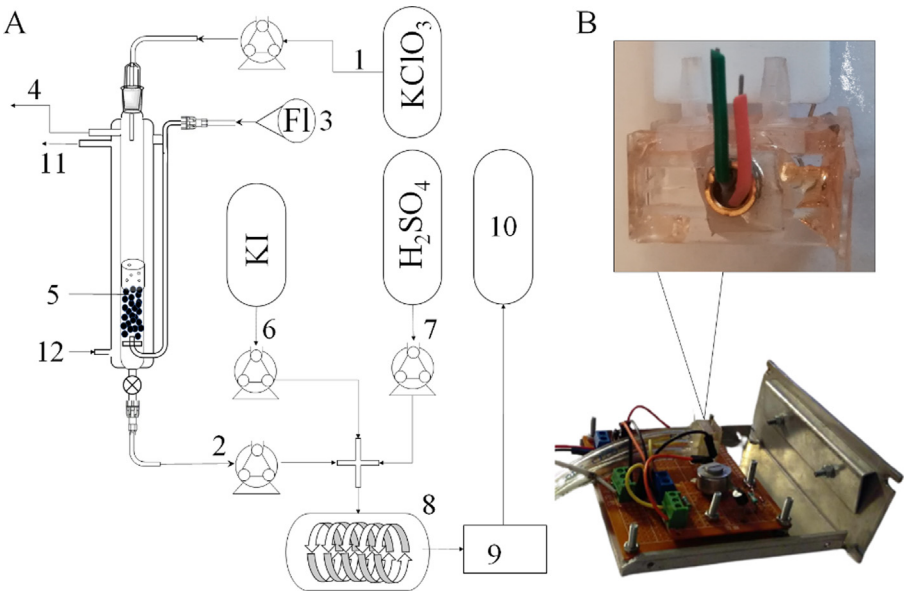

Fig. 1 (A) Schematic representation of the continuous chlorate hydrogenation set-up: 1) chlorate solution; 2) solution outlet; 3) H_2 flow inlet; 4) gas outlet; 5) catalyst; 6) KI solution; 7) H_2SO_4 solution; 8) thermostatic mixing loop; 9) spectrophotometric measuring cell; 10) waste collecting dish; 11) heating flow outlet; 12) heating flow inlet; (B) spectrophotometric measuring system.

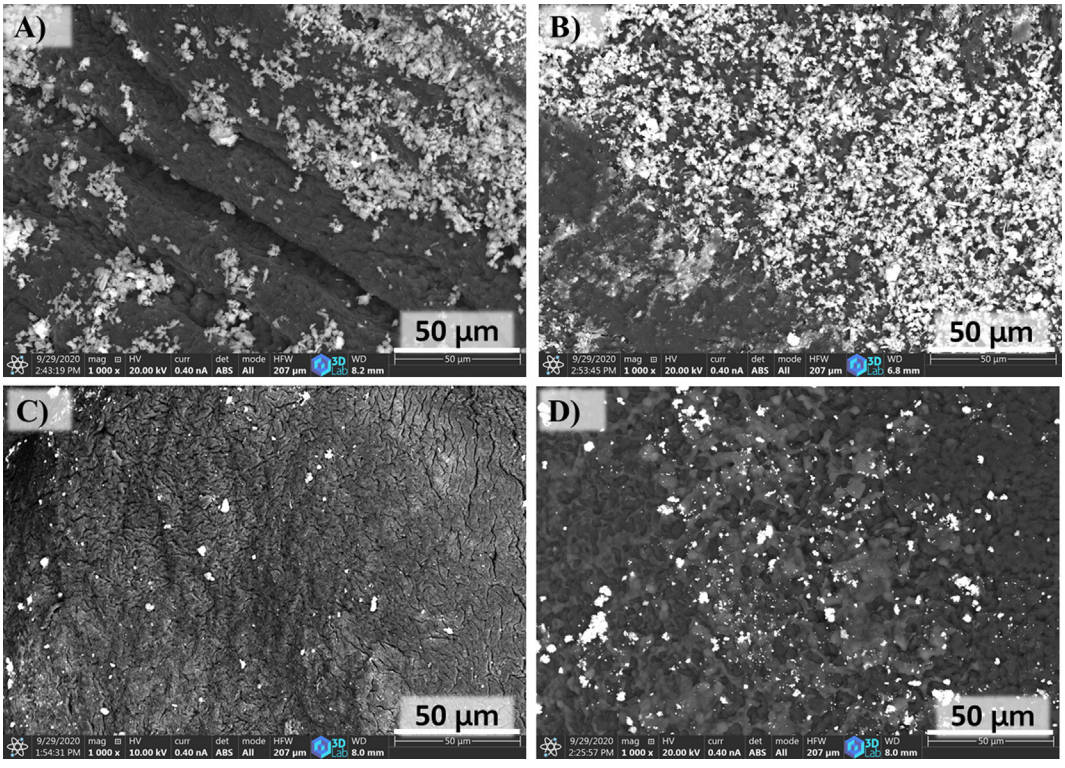

Fig. 2 SEM images of the designed cellulose-based catalysts: (A) Pd-Pt/CB-Fe_2O_3, (B) Pt-Pd/CB-Fe_2O_3, (C) Pd-Pt/CB, (D) Pt-Pd/CB.

The XRD analysis (Fig. 3.) confirmed that elemental palladium nanoparticles present in the sample, as the peaks found at 40.0° and 45.9° 2Θ angles can be identified as Pd (111) and Pd (200) reflexions (ICDD card number 046-1043). At 39.6° 2Θ degree another peak has been located which corresponds to the Pt (111) reflexion (ICDD card number 00-004-082). In case of the iron oxide containing catalysts, peaks at 24.1°, 33.2°, 35.6° 40.9°, 49.5°, 54.1°, 62.5°, and 64.0° 2Θ degrees have been found, which can be associated with the (012), (104), (110) (113), (024), (116), (214), and (208) reflexions of α-Fe_2O_3 (ICDD card number 33-0664). The wide peaks at 12.2°, 19.2° and 21.6° belongs to the (100), (110) and

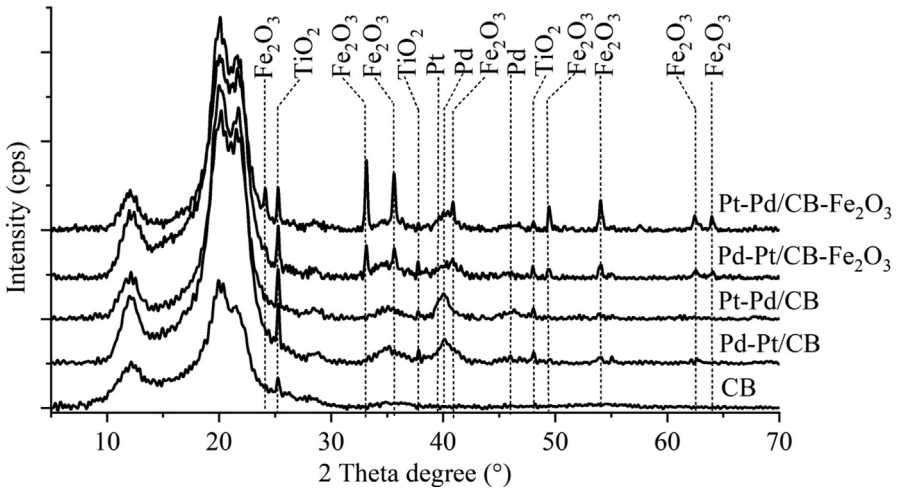

Fig. 3 XRD patterns of the designed catalysts and the applied cellulose beads.

(020) planes of cellulose (French, 2014). Anatase were also identified in the samples, as peaks at 25.3°, 37.8°, and 48.0° 2Θ degrees have been appeared (ICDD card number 21-1272) which corresponds to (101), (004), and (200) reflexions of TiO_2. The presence of anatase can be explained by the production method of the cellulose beads, because TiO_2 is the most widely used solid matrix (principal pillar supporting) during the adsorption of the epichlorohydrin in the initial step of cellulose production (Lei et al., 2003).

FTIR measurements were also performed to identify the surface functional groups of the catalysts. These are important because appropriate groups could promote the adsorption of noble metals on the surface through ion exchange adsorption, electrostatic interactions, and complex formation. There is no significant difference between the coverage of the surface of the catalysts (Fig. 4.). The wide band located between 3100 cm^{-1} and 3500 cm^{-1} indicates the presence of —OH stretching (Maaloul et al., 2020; Yang et al., 2007). The peak at 2888 cm^{-1} can be associated with C—H stretching (Jiang et al., 2017; Yang et al., 2007; Zhang et al., 2018). The band at 1643 cm^{-1} indicates C═C vibration occur, but only in case of the pure cellulose beads (CB) (Yang et al., 2007). At 1371 cm^{-1} a peak indicating O—H bending vibration in each sample (Mazlan et al., 2019). Strong peaks about 1000 and 1200 cm^{-1} corresponds to C—O and C—O—C groups (Maaloul et al., 2020; Zhang et al., 2018). The peak at 895 cm^{-1} belongs to C—H bending vibration (Szymanska-Chargot and Zdunek, 2013), while the Fe_2O_3 containing samples show bands about 541 cm^{-1}, which are related to Fe—O stretching (Alves et al., 2019).

The palladium, platinum and iron contents of the catalysts were determined by using ICP (Table 1). The Pt-Pd/CB catalyst contain ~1.4 times more precious metal than its iron oxide promoted counterpart, Pt-Pd/CB-Fe_2O_3. There is no significant difference in the minor precious metal content of the catalysts with or without promoter.

All four catalysts were tested in chlorate hydrogenation using a batch set-up. Better results have been obtained by using the iron oxide promoted samples during the hydrogenation (Fig. 5, A). The highest activity was achieved with the Pd-Pt/CB-Fe_2O_3 catalyst, and it reduced the initial chlorate

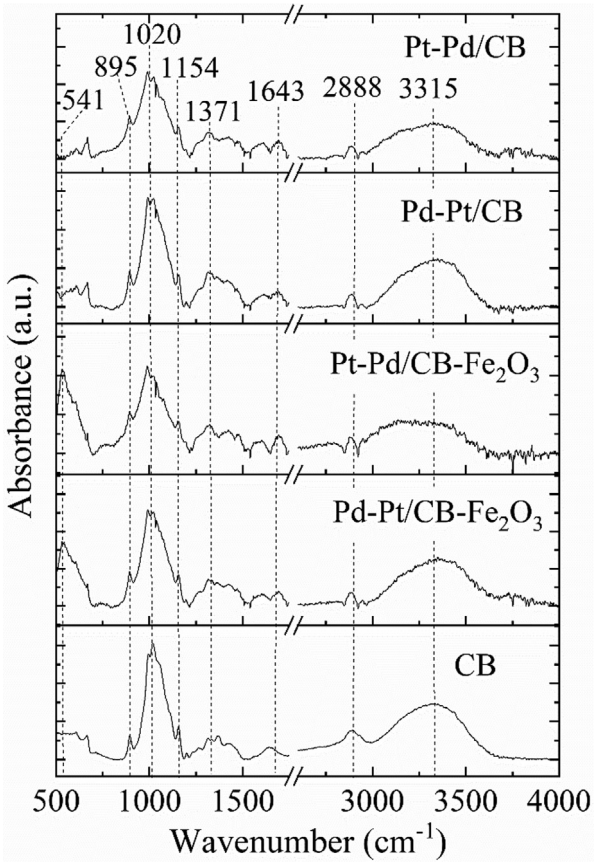

Fig. 4 FTIR spectra of the designed catalysts and the applied cellulose beads.

concentration from 200 mg/L to ~15 mg/L (Fig. 5, A). The other three catalysts, Pt-Pd/CB-Fe_2O_3, Pd-Pt/CB and Pt-Pd/CB were also efficient, but the remaining chlorate concentrations after 3 h hydrogenation were much higher, about 30, 53, and 48 mg/L, respectively. Catalytic tests were also performed with cellulose beads containing iron oxide and with unsupported Fe_2O_3 (SI Fig. 3), but no significant activity

Table 1 Pd, Pt, and Fe content of the developed catalysts.

Catalyst	Pd	Pt	Fe
	wt%		
Pd-Pt/CB	0.31	0.03	–
Pt-Pd/CB	0.09	0.56	–
Pd-Pt/CB-Fe_2O_3	0.43	0.05	1.25
Pt-Pd/CB-Fe_2O_3	0.07	0.38	1.01
Pd-Pt/CB-Fe_2O_3 (5x used)	0.26	0.023	0.31

was observed. To the best of our knowledge, the role of Fe_2O_3 in the case of chlorate hydrogenation has not been studied before. However, it was found that iron oxide promote the fast and effective adsorption/desorption of reactants and products on the surface of catalysts (Tang et al., 2021; Xu et al., 2021). It has also been observed for Pt or Pd-containing catalysts that Fe_2O_3 promotes oxygen adsorption and water formation which is advantageous in dehydrogenation processes such as chlorate reduction (Hensley et al., 2014; Li et al., 2021).

In our previous study (Sikora et al., 2020), commercially available palladium-containing catalysts have been examined in the hydrogenation of chlorate ions. The best Pd/C catalyst achieved 93% conversion under the same conditions. Although in that case less (200 mg) catalyst was used for the hydrogenation, but the noble metal content (10 wt%) of the tested commercially available catalysts was higher. The synthesized Pd-Pt/CB-Fe_2O_3 catalyst could achieve the same conversion with a lower metal content, furthermore, the Pd/C catalysts could not be tested and applied in a flow-through system due to their powder-based form.

By applying the cellulose beads supported Pd-Pt bimetallic catalyst, the hydrogenation reaction occurs according to a pseudo-first-order kinetics, which was verified by linear regression on the initial measurement points of the ln c_{NB} *vs.* reaction time plot (Fig. 5, C). The reaction rate constants (k) were determined by applying linear regression using Eq. (3) as follows:

$$\ln\left(c_{ClO_3^-}\right) = -kt + \ln(c_{0\,ClO_3^-}) \tag{3}$$

where $c_{ClO_3^-}$ is the chlorate concentration in mol/dm^3, k is the rate constant (s^{-1}) and t is time (s). In case of both iron(III) oxide free bimetallic catalysts, the rate constants are similar (Fig. 5. C). The promoter effect of the iron oxide was increasingly prevailed in case of the Pd-Pt/CB-Fe_2O_3 system, because the k value was significantly higher compared to the corresponding Fe_2O_3 free catalyst. However, the catalytic activity

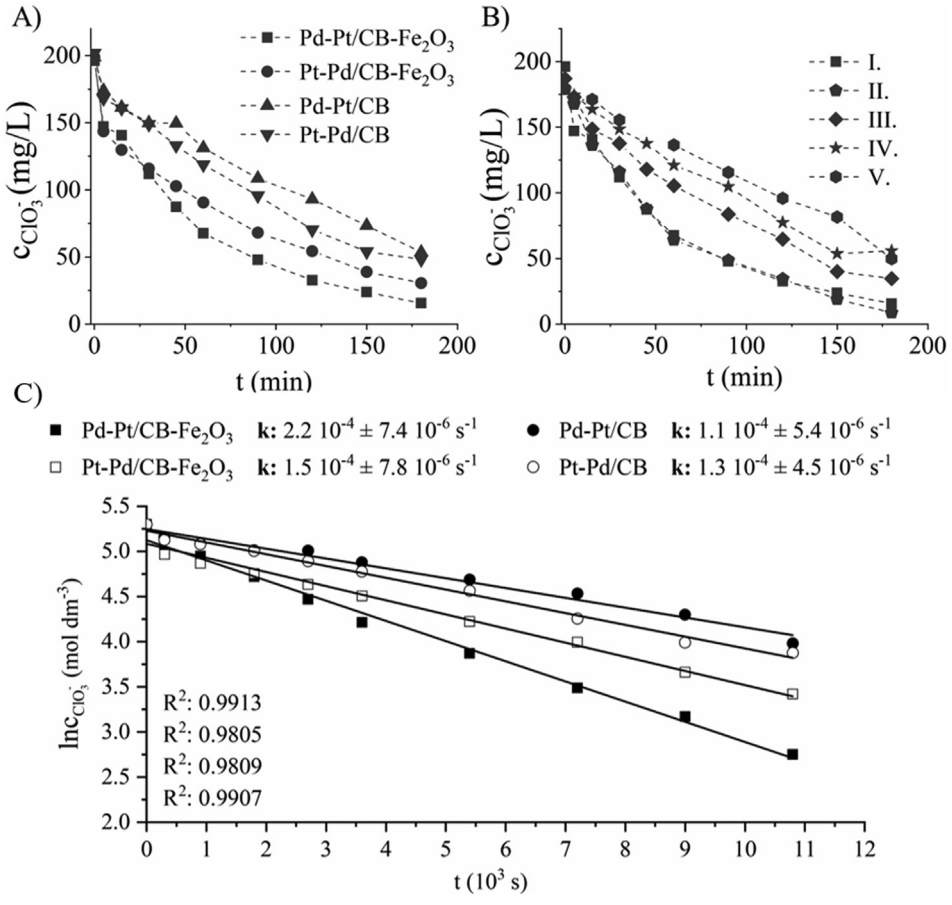

Fig. 5 (A) Comparison of the catalytic activity of the cellulose based catalysts with different Pd and Pt contents, and with or without Fe_2O_3 promoter in batch chlorate reduction experiments. (B) Reuse tests were also performed with the most active catalyst (Pd-Pt/CB-Fe_2O_3) for five cycles. (C) The lnc *vs* t diagram with the corresponding calculated k values of chlorate hydrogenation carried out in the presence of the different catalysts.

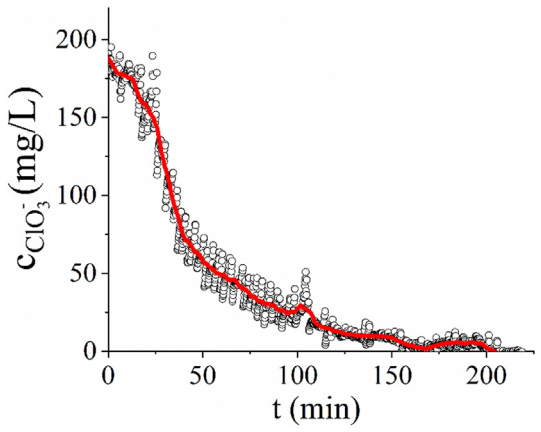

Fig. 6 Catalytic activity of the Pd-Pt/CB-Fe_2O_3 catalyst in a chlorate hydrogenation experiment performed in a continuous flow set-up.

of the Pt-Pd/CB-Fe_2O_3 system did not improved compared to its iron(III) oxide free counterpart.

Reuse tests were also performed with the most active catalyst (Pd-Pt/CB-Fe_2O_3) for 4 more cycles (Fig. 5/B. There is no significant difference between the first two hydrogenations, however with further uses the amount of reduced chlorate starts to decrease slightly. After the 5th hydrogenation cycle about 3 times more chlorate (50 mg/L) remained than in the first cycle.

The decrease in catalytic activity after the cycles, is caused by metal leaching (ICP results, Table 1.). Based on the ICP results, the metal loss is high, although the catalytic activity is still reasonable compared to the metal loss. In order to prevent metal leaching, the surface of the cellulose can be modified to increase its adsorption capacity and thus, the binding of the precious metal particles to create more stable catalysts (Hokkanen et al., 2016).

The most promising catalyst, Pd-Pt/CB-Fe_2O_3 was also tested in a continuous flow system (Fig. 6). The hydrogenation was monitored for more than 3 h, and the chlorate concentration decreased continuously over time and then reduced to 0 in about 160 min.

4. Conclusion

Cellulose bead supported palladium and platinum catalysts have been successfully designed and prepared. The size of the noble metal particles is <10 nm. The catalysts have low specific surface area (<1 m^2/g) and low precious metal content (<0.6 wt%), however they showed excellent catalytic activity in the hydrogenation of chlorate. The effect of iron oxide promoter material is also tested. Although the Pd-Pt/CB catalyst achieved only 72% conversion, the addition of iron oxide to the system increased this by more than 20% in a batch set-up. The Pd-Pt/CB-Fe_2O_3 catalyst was successfully applied in a continuous hydrogenation process, and within 160 min it was able to reduce the chlorate concentration to zero.

Declaration of Competing Interest

The authors declare that they have no known competing financial interests or personal relationships that could have appeared to influence the work reported in this paper.

Acknowledgements

The authors thank Tibor Ferenczi (Institute of Metallurgy, University of Miskolc) for the BET measurements and Dr. Dániel Koncz-Horváth (Higher Education Industry Cooperation Centre, University of Miskolc) along with the 3DLab (University of Miskolc) for the SEM images.

The article was prepared with the professional support of the Doctoral Student Scholarship Program of the Co-operative Doctoral Program of the Ministry of Innovation and Technology financed from the National Research, Development and Innovation Fund. The described article was carried out as part of the EFOP-3.6.1-16-2016-00011 "Younger and Renewing University – Innovative Knowledge City – institutional development of the University of Miskolc aiming at intelligent specialisation" project implemented in the framework of the Szechenyi 2020 program. The realization of this project is supported by the European Union, co-financed by the European Social Fund.

Appendix A. Supplementary data

Supplementary data to this article can be found online at https://doi.org/10.1016/j.arabjc.2021.103202.

References

Akhtar, F., Andersson, L., Ogunwumi, S., Hedin, N., Bergström, L., 2014. Structuring adsorbents and catalysts by processing of porous powders. J. Eur. Ceram. Soc. 34, 1643–1666. https://doi.org/10.1016/j.jeurceramsoc.2014.01.008.

Alves, I.C.B., Santos, J.R.N., Viégas, D.S.S., Marques, E.P., Lacerda, C.A., Zhang, L., Zhang, J., Marques, A.L.B., 2019. Nanoparticles of Fe2O3 and Co3O4 as efficient electrocatalysts for oxygen reduction reaction in acid medium. J. Braz. Chem. Soc. 30, 2681–2690 https://doi.org/10.21577/0103-5053.20190195.

Bahsis, L., El Ayouchia, H. Ben, Anane, H., Benhamou, K., Kaddami, H., Julve, M., Stiriba, S.E., 2018. Cellulose-copper as bio-supported recyclable catalyst for the clickable azide-alkyne [3 + 2] cycloaddition reaction in water. Int. J. Biol. Macromol. 119, 849–856. https://doi.org/10.1016/j.ijbiomac.2018.07.200.

Brinkmann, T., Giner Santonja, G., Schorcht, F., Roudier, S., Delgado Sancho, L., 2014. Best Available Techniques Reference Document for the Production of Chlor-alkali. https://doi.org/10.2791/13138.

Chen, X., Huo, X., Liu, J., Wang, Y., Werth, C.J., Strathmann, T.J., 2017. Exploring beyond palladium: Catalytic reduction of aqueous oxyanion pollutants with alternative platinum group metals and new mechanistic implications. Chem. Eng. J. 313, 745–752. https://doi.org/10.1016/j.cej.2016.12.058.

Dong, Y., Bi, J., Zhang, S., Zhu, D., Meng, D., Ming, S., Qin, K., Liu, Q., Guo, L., Li, T., 2020. Palladium supported on N-Heterocyclic carbene functionalized hydroxyethyl cellulose as a novel and efficient catalyst for the Suzuki reaction in aqueous media. Appl. Surf. Sci. 531,. https://doi.org/10.1016/j.apsusc.2020.147392 147392.

French, A.D., 2014. Idealized powder diffraction patterns for cellulose polymorphs. Cellulose 21, 885–896. https://doi.org/10.1007/s10570-013-0030-4.

Gurol, M., Kim, K., 2003. Perchlorate removal methods. US10/023,573.

Hensley, A.J.R., Hong, Y., Zhang, R., Zhang, H., Sun, J., Wang, Y., McEwen, J.S., 2014. Enhanced Fe2O3 reducibility via surface modification with Pd: Characterizing the synergy within Pd/Fe catalysts for hydrodeoxygenation reactions. ACS Catal. 4, 3381–3392. https://doi.org/10.1021/cs500565e.

Hokkanen, S., Bhatnagar, A., Sillanpää, M., 2016. A review on modification methods to cellulose-based adsorbents to improve adsorption capacity. Water Res. https://doi.org/10.1016/j.watres.2016.01.008.

Hosseini, S., Moghaddas, H., Masoudi Soltani, S., Kheawhom, S., 2020. Technological Applications of Honeycomb Monoliths in Environmental Processes: A review. Process Saf. Environ. Prot. https://doi.org/10.1016/j.psep.2019.11.020

Jakab-Nácsa, A., Stomp, D., Farkas, L., Kaptay, G., 2020. Large NaCl-Effect on the Decomposition Rate of Chlorate Ions in HCl-Containing Brine Solutions and Its Consequences for the Chlor-Alkali Industry. Period. Polytech. Chem. Eng. 65, 238–242. https://doi.org/10.3311/ppch.14634.

Jiang, X., Wang, S., Ge, L., Lin, F., Lu, Q., Wang, T., Huang, B., Lu, B., 2017. Development of organic-inorganic hybrid beads from sepiolite and cellulose for effective adsorption of malachite green. RSC Adv. 7, 38965–38972. https://doi.org/10.1039/c7ra06351b.

Kuznetsova, L.I., Kuznetsova, N.I., Koscheev, S.V., Zaikovskii, V.I., Lisitsyn, A.S., Kaprielova, K.M., Kirillova, N.V., Twardowski, Z., 2012. Carbon-supported iridium catalyst for reduction of chlorate ions with hydrogen in concentrated solutions of sodium chloride. Appl. Catal. A Gen. 427–428, 8–15. https://doi.org/10.1016/j.apcata.2012.03.024.

Lei, Y.L., Lin, D.Q., Yao, S.J., Zhu, Z.Q., 2003. Preparation and characterization of titanium oxide-densified cellulose beads for expanded bed adsorption. J. Appl. Polym. Sci. 90, 2848–2854. https://doi.org/10.1002/app.13010.

Li, D. Dan, Lu, G. Ping, Cai, C., 2020. Modified cellulose with tunable surface hydrophilicity/hydrophobicity as a novel catalyst support for selective reduction of nitrobenzene. Catal. Commun. 137, 105949. https://doi.org/10.1016/j.catcom.2020.105949

Li, D.D., Zhang, J.W., Cai, C., 2018. Pd Nanoparticles Supported on Cellulose as a Catalyst for Vanillin Conversion in Aqueous Media. J. Org. Chem. 83, 7534–7538. https://doi.org/10.1021/acs.joc.8b00246.

Li, W., Liu, R., Kang, H., Sun, Y., Dong, F., Huang, Y., 2013. Synthesis of amidoxime functionalized cellulose derivatives as a reducing agent and stabilizer for preparing gold nanoparticles. Polym. Chem. 4, 2556–2563. https://doi.org/10.1039/c3py00052d.

Li, Z., Dai, S., Ma, L., Qu, Z., Yan, N., Li, J., 2021. Synergistic interaction and mechanistic evaluation of NO oxidation catalysis on Pt/Fe2O3 cubes. Chem. Eng. J. 413,. https://doi.org/10.1016/j.cej.2020.127447 127447.

Lin, X., Wu, M., Wu, D., Kuga, S., Endo, T., Huang, Y., 2011. Platinum nanoparticles using wood nanomaterials: Eco-friendly synthesis, shape control and catalytic activity for p-nitrophenol reduction. Green Chem. 13, 283–287. https://doi.org/10.1039/c0gc00513d.

Lucchini, M.A., Lizundia, E., Moser, S., Niederberger, M., Nyström, G., 2018. Titania-Cellulose Hybrid Monolith for In-Flow Purification of Water under Solar Illumination. ACS Appl. Mater. Interfaces 10, 29599–29607. https://doi.org/10.1021/acsami.8b09735.

Maaloul, N., Oulego, P., Rendueles, M., Ghorbal, A., Díaz, M., 2020. Synthesis and characterization of eco-friendly cellulose beads for copper (II) removal from aqueous solutions. Environ. Sci. Pollut. Res. 27, 23447–23463. https://doi.org/10.1007/s11356-018-3812-2.

Maslamani, N., Khan, S.B., Danish, E.Y., Bakhsh, E.M., Zakeeruddin, S.M., Asiri, A.M., 2020. Carboxymethyl cellulose nanocomposite beads as super-efficient catalyst for the catalytic reduction of organic and inorganic pollutants. Int. J. Biol. Macromol. https://doi.org/10.1016/j.ijbiomac.2020.11.074

Mazlan, N.S.N., Zakaria, S., Gan, S., Hua, C.C., Baharin, K.W., 2019. Comparison of regenerated cellulose membrane coagulated in sulphate based coagulant. Cerne 25, 18–24. https://doi.org/10.1590/01047760201925012586.

Nasrollahzadeh, M., Shafiei, N., Nezafat, Z., Soheili Bidgoli, N.S., Soleimani, F., 2020. Recent progresses in the application of cellulose, starch, alginate, gum, pectin, chitin and chitosan based (nano)catalysts in sustainable and selective oxidation reactions: A review. Carbohydr. Polym. https://doi.org/10.1016/j.carbpol.2020.116353.

Quignard, F., Choplin, A., 2001. Cellulose: A new bio-support for aqueous phase catalysts. Chem. Commun. 21–22. https://doi.org/10.1039/b007776n.

Ren, C., Yang, P., Gao, J., Huo, X., Min, X., Bi, E.Y., Liu, Y., Wang, Y., Zhu, M., Liu, J., 2020. Catalytic Reduction of Aqueous Chlorate with MoO xImmobilized on Pd/C. ACS Catal. 10, 8201–8211. https://doi.org/10.1021/acscatal.0c02242.

Rutger, V.S., Klesing, A., Neuenfeldt, G., Ottmann, A., 2001. Method for removing chlorate ions from solutions. US6270682.

Sikora, E., Karacs, G., Kocserha, I., Muránszky, G., Fiser, B., Viskolcz, B., Vanyorek, L., 2020. Hydrogenation of chlorate ions by commercial carbon supported palladium catalysts—a comparative study. React. Kinet. Mech. Catal. 1–9. https://doi.org/10.1007/s11144-020-01829-1.

Szymanska-Chargot, M., Zdunek, A., 2013. Use of FT-IR Spectra and PCA to the Bulk Characterization of Cell Wall Residues of Fruits and Vegetables Along a Fraction Process. Food Biophys. 8, 29–42. https://doi.org/10.1007/s11483-012-9279-7.

Tan, J., Liu, R., Wang, W., Liu, W., Tian, Y., Wu, M., Huang, Y., 2010. Controllable aggregation and reversible pH sensitivity of AuNPs regulated by carboxymethyl cellulose. Langmuir 26, 2093–2098. https://doi.org/10.1021/la902593e.

Tang, X., Wang, J., Li, J., Zhang, X., La, P., Jiang, X., Liu, B., 2021. In-situ growth of large-area monolithic Fe2O3/TiO2 catalysts on flexible Ti mesh for CO oxidation. J. Mater. Sci. Technol. 69, 119–128. https://doi.org/10.1016/j.jmst.2020.08.026.

Tavker, N., Gaur, U., Sharma, M., 2020. Cellulose supported bismuth vanadate nanocomposite for effective removal of organic pollutant. J. Environ. Chem. Eng. 8,. https://doi.org/10.1016/j.jece.2020.104027 104027.

WHO, 2005. Chlorite and chlorate in drinking- water. WHO Guidel. Drink. Water Qual. 31.

Wu, X., Lu, C., Zhang, W., Yuan, G., Xiong, R., Zhang, X., 2013. A novel reagentless approach for synthesizing cellulose nanocrystal-supported palladium nanoparticles with enhanced catalytic performance. J. Mater. Chem. A 1, 8645–8652. https://doi.org/10.1039/c3ta11236e.

Wu, X., Lu, C., Zhou, Z., Yuan, G., Xiong, R., Zhang, X., 2014. Green synthesis and formation mechanism of cellulose nanocrystal-supported gold nanoparticles with enhanced catalytic performance. Environ. Sci. Nano 1, 71–79. https://doi.org/10.1039/c3en00066d.

Xie, Z.T., Asoh, T.A., Uetake, Y., Sakurai, H., Uyama, H., 2020. Dual roles of cellulose monolith in the continuous-flow generation and support of gold nanoparticles for green catalyst. Carbohydr. Polym. 247. https://doi.org/10.1016/j.carbpol.2020.116723.

Xie, Z.T., Asoh, T.A., Uyama, H., 2019. Monolithic cellulose supported metal nanoparticles as green flow reactor with high catalytic efficiency. Carbohydr. Polym. 214, 195–203. https://doi.org/10.1016/j.carbpol.2019.03.036.

Xu, W., Xue, W., Huang, H., Wang, J., Zhong, C., Mei, D., 2021. Morphology controlled synthesis of α-Fe2O3-x with benzimidazole-modified Fe-MOFs for enhanced photo-Fenton-like catalysis. Appl. Catal. B Environ. 291,. https://doi.org/10.1016/j.apcatb.2021.120129 120129.

Yang, H., Yan, R., Chen, H., Lee, D.H., Zheng, C., 2007. Characteristics of hemicellulose, cellulose and lignin pyrolysis. Fuel 86, 1781–1788. https://doi.org/10.1016/j.fuel.2006.12.013.

Yilmaz, B., Müller, U., 2009. Catalytic applications of zeolites in chemical industry. In: Topics in Catalysis. Springer, pp. 888–895. https://doi.org/10.1007/s11244-009-9226-0.

Zhang, S., Zhang, F., Pan, Y., Jin, L., Liu, B., Mao, Y., Huang, J., 2018. Multiwall-carbon-nanotube/cellulose composite fibers with enhanced mechanical and electrical properties by cellulose grafting. RSC Adv. 8, 5678–5684. https://doi.org/10.1039/c7ra11304h.